Nat. Hazards Earth Syst. Sci. Discuss., https://doi.org/10.5194/nhess-2017-285
Manuscript under review for journal Nat. Hazards Earth Syst. Sci.
Discussion started: 7 September 2017

Natural Hazards and Earth System Sciences
Discussions

Physically based approaches incorporating evaporation for early warning predictions of rainfall-induced landslides

Alfredo Reder[1,2], Guido Rianna[2], Luca Pagano[1]

[1]Department of Civil, Architectural and Environmental Engineering, University of Naples Federico II, Naples, 80125, Italy
[2]Regional Models and geo-Hydrological Impacts Division, CMCC Foundation, Capua, 81043, Italy

Correspondence to: Guido Rianna (guido.rianna@cmcc.it)

Abstract. In the field of rainfall-induced landslides on sloping covers, models for early warning predictions require an adequate trade-off between two aspects: prediction accuracy and promptness. When a cover's initial hydrological state is a determining factor in triggering landslides, taking evaporative losses into account (or not) could significantly affect both aspects. This study evaluates the performance of three physically based predictive models, converting precipitation and evaporation fluxes into hydrological variables useful in assessing slope safety conditions. Two of the models incorporate evaporation, with one representing evaporation as both a boundary and internal phenomenon, and the other only a boundary phenomenon. The third model totally disregards evaporation. Model performances are assessed by analysing a well-documented case study involving a two-meter thick sloping volcanic cover. The large amount of monitoring data collected for the soil involved in the case study, reconstituted in a suitably equipped lysimeter, makes it possible to propose procedures for calibrating and validating the parameters of the models. All predictions indicate a hydrological singularity at the landslide time (alarm). Comparison of the models' predictions also indicates that the greater the complexity and completeness of the model, the lower the number of predicted hydrological singularities when no landslides occur (false alarms).

1 Introduction

In Italy, several slopes made of sand or silty sand covers experience unsaturated conditions throughout the hydrological year, founding part of their stability conditions on strength provided by suction, especially when slope angles exceed friction angles. The sequence of rainfall events occurring over the wet season induces a general reduction in suction levels, increasing the cover's susceptibility to an exceptional rainfall event. On the other hand, evaporation fluxes reduce susceptibility to sliding by increasing suction levels. The antecedent period, during which the contrast between rainfall and evaporation affects suction levels, may last weeks or months depending on the hydraulic properties of the soils involved and the climate regime of the area.

The 2005 Nocera Inferiore landslide [hereinafter "2005NIL"] was interpreted (Pagano et al., 2010) by merely referring to precipitation recorded by a meteorological station placed near the landslide area (Fig. 1). Richards' equation (1931) in 1-D flow conditions was adopted to convert hourly precipitation records into the evolution of soil suction at various depths. This

simple approach highlighted the crucial role of antecedent rainfalls (945 mm of rainfall over 4.5 months), which had reduced soil suction to very low values before the occurrence of the major event (143 mm of rainfall over 16 hours). Analysis results indicated in suction vanishing throughout the cover the triggering cause. Virtual scenarios built with modified antecedent rainfalls were analysed, and they indicated that the phenomenon would have not occurred if the antecedent periods had been drier. The crucial factor affecting soil suction at triggering time was the weather conditions over the previous four months.

A meteorological window of such long influence implies that it would not be reasonable to neglect evaporation fluxes, as their persistency could result in significant drying processes even during the cold season, when evaporation is at its lowest (about 1-2 mm/day in winter). Rianna et al. (2014a) measured infiltrating precipitation and actual evaporation induced by the actual weather conditions on a layer placed in a lysimeter, made using the same soil that was involved in the 2005NIL. Monitoring showed that the amounts of actual evaporation and infiltrating precipitation over a hydrological year occur to the same order of magnitude (hundreds of millimeters).

Increasing efforts are being made to develop early warning systems to mitigate the risks of rainfall-induced landslides. Their success strongly depends on the performance of the predictive models they implement in terms of timing and accuracy of prediction.

In the context of physically based predictive models, some widely-adopted approaches implemented up to now (Iverson, 2000; Montgomery and Dietrich, 1994; Baum et al., 1998; Liao et al., 2011; Formetta et al., 2014; Teixeira et al., 2015) usually neglect evaporation effects. There are a number of reasons for this neglect, all essentially related either to a belief that evapotranspiration exerts little influence or to difficulties and uncertainties arising when a boundary value problem incorporating evapotranspiration is to be solved. However, such assumption can result reasonable only for thin and/or highly pervious soil covers (Brand et al., 1984; Chatterjea, 1989; Morgenstern, 1992). In principle, modelling evaporation requires approaches coupling water and heat flows. Geotechnical engineers and geologists are still too unfamiliar with heat flow modelling in particular, as it entails a number of thermal parameters and boundary conditions that are difficult to calibrate and validate. In addition, governing equations need non-widespread numerical codes while, at the same time, high non-linearity involves significant efforts to achieve numerical solutions.

The question naturally arises whether the accuracy of the early warning prediction will be significantly reduced if evaporation is neglected, resulting in too many false alarms. The study attempts to address this by comparing results yielded by three different models, either taking evaporation into account or neglecting it, in the interpretation of the 2005NIL case study.

For this study, in addition to hourly precipitation values, the availability of air relative humidity and air temperature records makes it possible to estimate the evaporative fluxes potentially experienced by the cover involved in the landslide, complementing precipitation in characterizing the fluxes that have affected the hydrological state of the cover over time. Two of the models account for evaporation: one based on a coupled (heat-water flow) approach, and the other based on an isothermal approach. The third model neglects evaporation entirely. It represents an update to the approach previously adopted in Pagano et al. (2010). Suction and other hydrological variables predicted by using all the selected models are presented and discussed in an attempt to characterize their various performances.

Since models are presumed to be operating in real time, namely receiving recorded meteorological variables as input data and returning variables relating to slope safety conditions as output data, they need to be applied to simplified geometrical and mechanical patterns to save as much analysis time as possible. The paper also discusses which simplifications are able to accelerate predictions without excessively reducing accuracy of prediction.

Considerable effort has been made in this study to develop procedures for calibrating model parameters, and they are based on the interpretation of the experimental results provided by the above-mentioned lysimeter.

The paper begins with a description of the case study and presents the lysimeter data. After describing the selected models and simplifications carried out to save analysis time, it illustrates all the procedures followed to calibrate the parameters. Lastly, it presents and compares the results of the analyses, discussing model performance from the point of view of their possible use as early warning predictors.

2 Methods

2.1 Field experimental data: the Nocera Inferiore 2005 landslide

2005NIL involved a triangular shaped area of 24,600 m^2 and a soil mass of 33,000 m^3 covering a 36° open slope (Fig. 1c). In the uppermost part of the landslide, in the triggering zone, the slope angle approaches 39° (de Riso et al., 2007) and the pyroclastic cover is made up of 2 m thick loose non-plastic silty sand (volcanic ash) (Fig. 2). The bedrock consists of highly fractured limestone located at a depth ranging from 1 to 2 m, approaching the maximum values at the apical zone.

The landslide triggered in the apical zone, spreading downward. The rapid post-failure movement caused the death of three people whose house was destroyed by the impact of the soil mass, which then covered a wide area (20,000 m^2) at the toe of the slope (Fig. 1c). In the same zone, two smaller landslides occurred less than 1 km from the main one at the same time.

Figure 3 plots the evolution of precipitation (Pagano et al., 2010) and other atmospheric variables at the landslide site over a time span of about ten years (1998-2008), including the investigated landslide (4 March 2005) in the second part. Changes in daily air temperature (Fig. 3a) and air relative humidity (Fig. 3b) are used to estimate the daily potential evaporation (Fig. 3d) by following the FAO guidelines (Allen et al., 1998). The potential evaporation intensities occur much lower than precipitation intensities (Fig. 3c). However, potential evaporation persistency makes cumulated values (Fig. 3e) significant even during winter, when the flux is minimum.

Figure 3e shows that the hydrological year in which the landslide took place is associated with the highest cumulated precipitation. The most significant spread between cumulated values of precipitation (1200 mm) and potential evaporation (380 mm) is observed (see vertical segment with rows in Fig. 3e) at the time of the landslide.

2.2 Experimental data provided by the physical model

An extensive description of the physical model and the experimental data obtained may be found in Rianna et al. (2014a, b). A wooden tank (Fig. 4) houses a 0.75 m thick layer of non-plastic sandy-silt volcanic soil. This soil was selected and placed

in such a way as to try to reproduce the intrinsic properties and field porosities (around 70%) of the material involved in 2005NIL (Fig. 2). A geotextile bounds the bottom of the layer. It acts as a capillary barrier as its voids are larger than those of the overlying soil (Reder et al., 2017). The behaviour at the bottom should therefore be consistent with that of fractured bedrock with partly empty fractures or a gravel layer (pumice).

The monitoring scheme implemented in the physical model (Fig. 4) makes it possible to obtain potential fluxes (total precipitation and potential evaporation), actual fluxes developing across the uppermost layer surface (actual evaporation and infiltrated precipitation), and the effects induced by these fluxes within the layer (suction, volumetric water content, temperature). Fluxes are quantified by a meteorological station, the continuous weighting of the layer by three load cells sustaining the tank and sensors measuring all the energetic terms involved in the energy exchanges between soil and atmosphere (radiometer, pyrometer, heat flux plate, thermistors). Matric suctions (by jet-fill tensiometers and heat dissipation probes), volumetric water contents (using TDRs), and soil temperatures (using thermistors) are monitored at four depths within the layer.

The physical model was exposed to the atmosphere over four hydrological years in bare conditions, and it returned a number of behavioural patterns for the evolution of the layer's hydrological and thermal states. These patterns suggest the ingredients that a predictive model should include, allow quantification of soil properties, and they ultimately represent a useful reference framework against which to compare predictions in order to assess their reliability.

The reference behavioural pattern considered here is represented by the evolution of water storage (WS) in the layer (Fig. 5), soil suction (at two depths – Fig. 6a), and temperature (three depths – Fig. 7) over four hydrological years.

WS (Rianna et al., 2014a), expressed in terms of overall water volume in the layer divided by the layer surface (Fig. 5a), increases at the onset of wet periods due to precipitation (Fig. 5b) infiltrating the layer. For prolonged wet periods, such as those occurring during the first, third, and fourth years, WS tends to stabilize at a wet level (Fig. 5a, "wet threshold" line) placed just below the maximum saturation value in the layer (Fig. 5a, "saturation" line). Above this wet level, drainage is often observed during, and immediately after, rainfall events, whereas drainage has never been observed below it. During dry periods, water storage decreases due to evaporation (Fig. 5c), and during prolonged dry periods it tends to reach a minimum at the dry threshold.

Soil suction (Fig. 6a) measured at different depths is consistent with water storage evolution (Rianna et al., 2014a). It progressively increases during the dry period, resulting in asynchronous fluctuations, indicating a slow propagation through the sample of changes in the atmospheric conditions. Suction values exceed the jet-fill tensiometer full scale during the summer periods, but reduce to few kPa during the wet season, resulting in this case in synchronous fluctuations, in line with prompt propagation throughout the layer of changes in boundary conditions determined by the atmosphere.

Temperature (Fig. 7) measured at the four depths follows an evolution consistent with atmospheric temperature (Rianna et al., 2014a). Fluctuations in the temperature of the atmosphere tend to reduce as depth increases due to greater soil filter action.

Nat. Hazards Earth Syst. Sci. Discuss., https://doi.org/10.5194/nhess-2017-285
Manuscript under review for journal Nat. Hazards Earth Syst. Sci.
Discussion started: 7 September 2017

2.3 Predictive models

Three different models were selected to convert the meteorological evolution (Fig. 3) recorded at the landslide area into hydrological variables for the cover. Shared features are:

- the one-dimensionality of water fluxes; this hypothesis, formulated in order to save analysis time in early warning applications, should also lead to realistic estimations of the hydrological state of the cover in line with indications for similar soils provided by interpreting field measurements (Pirone et al., 2015) and theoretical studies (Pagano et al., 2010);
- the rigidity of the domain; neglecting the effects of deformational processes induced by suction changes is suggested by the stiff volumetric response observed under swelling-reloading paths, which should speed up re-equilibrium processes so that hydraulic response is unaffected by the consolidation delay;
- precipitation history applied with hourly resolution at the top boundary; an incoming flux corresponding to rainfall intensity is applied at the top boundary in the meanwhile that at the same boundary the analysis returns pore water pressure values less than zero (atmospheric pressure); the top boundary condition is switched to null pore water to prevent pore water pressure from exceeding atmospheric pressure; this condition may be maintained until the analysis returns incoming fluxes less than rainfall intensity, otherwise it is again switched so that the incoming flux is equal to the rainfall intensity;
- surface seepage is applied at the bottom boundary; this condition corresponds to the hypothesis that the bedrock the volcanic layer rests on is intensely fractured and that the fractures are filled only by air (Reder et al., 2017).

The more comprehensive approach adopted couples the water balance equation with the heat balance equation and thermodynamic equilibrium (Wilson et al., 1994) and is applied using the Vadose/W code (GeoSlope, 2008).

The water balance equation is expressed as:

$$\frac{1}{\rho_w g}\frac{\partial(u_a-u_w)}{\partial t}=\frac{1}{\rho_w g m_2^w}\left[\frac{\partial}{\partial z}\left(k_w+\frac{k_w}{\rho_w g}\frac{\partial(u_a-u_w)}{\partial z}\right)+\left(\frac{P_a+u_v}{P_a\rho_w}\right)\frac{\partial}{\partial z}\left(D_v\frac{\partial u_v}{\partial z}\right)\right] \quad (1)$$

where u_w = liquid pore water pressure, u_a = pore air pressure, u_v = partial pressure of vapor pore water, m_2^w = slope of water soil characteristic curve, P_a = total atmospheric pressure, k_w = hydraulic conductivity function, D_v = function of vapor diffusivity through the soil, ρ_w = liquid water density, g = gravitational acceleration.

In comparison with the traditional form of water balance equation, describing the flow of liquid water through porous media, equation (1) contains an additional term (the second one in square brackets) taking into account the possibility of changes in the water phase.

The heat balance equation is expressed as:

Nat. Hazards Earth Syst. Sci. Discuss., https://doi.org/10.5194/nhess-2017-285
Manuscript under review for journal Nat. Hazards Earth Syst. Sci.
Discussion started: 7 September 2017

Natural Hazards and Earth System Sciences Discussions

$$C_h \frac{\partial T}{\partial t} = \frac{\partial}{\partial z}\left(\lambda \frac{\partial T}{\partial z}\right) - L_v \left(\frac{P_a + u_v}{P_a}\right) \frac{\partial}{\partial z}\left(D_v \frac{\partial u_v}{\partial z}\right) \quad (2)$$

where T = soil temperature, C_h = function of volumetric specific heat, λ = function of thermal conductivity, L_v = latent heat of water vaporization.

In this equation, the last term accounts for the amount of energy spent on water vaporization and represents the coupling with the water balance equation.

The thermodynamic equilibrium is expressed as:

$$u_v = u_{v0}\, exp\left(\frac{(u_a - u_w) M_w g}{RT}\right) \quad (3)$$

where u_{v0} = saturated partial pressure of pore vapour, M_w = water molecular weight, R = ideal gas constant.

The described model requires the following boundary conditions:

- soil suction $(u_a - u_w)_s$ or, alternatively, liquid water flux $(v_w)_s$ at the top-boundary; infiltrating precipitation was reproduced as already described in this section, and actual evaporation AE was reproduced according to the FAO approach described in what follows; u_a is assumed to be the same as the atmospheric pressure;

-vapor pressure $(u_v)_s$ or, alternatively, vapor water flux $(v_v)_s$; the boundary value problem was addressed by quantifying the former from air relative humidity RH and air temperature T_a records; RH provides the ratio $(u_v)_s/(u_{v0})_s$, while T_a provides the partial pressure of the vapor phase in saturated conditions $(u_{v0})_s$ using the Tetens equation (Tetens, 1930);

- temperature T_s is assumed to equal air temperature T_a measured two meters above the surface of the ground, in line with the approach followed by Wilson et al. (1997).

Actual evaporation AE is obtained as cut of Potential evaporation PE:

$$AE = k\, PE \quad (4)$$

according to the falling law proposed by Wilson et al. (1997):

$$k = \frac{exp\left(\frac{(u_a - u_w)_s M_w g}{RT_s}\right) - RH}{1 - RH} \quad (5)$$

and the PE expression of the FAO approach (Allen et al., 1998):

Nat. Hazards Earth Syst. Sci. Discuss., https://doi.org/10.5194/nhess-2017-285
Manuscript under review for journal Nat. Hazards Earth Syst. Sci.
Discussion started: 7 September 2017

Natural Hazards and Earth System Sciences Discussions

$$PE = k_{crop}\left[\frac{0.408\,\Gamma\,(R_n - G) + \eta\frac{900}{T_a + 273}u_{2m}\left(u_{v0}^{air} - u_v^{air}\right)}{\Gamma + \eta(1 + 0.34u_{2m})}\right] \quad (6)$$

where k_{crop} = crop coefficient, Γ = slope of the vapor pressure curve, R_n = net radiation flux, G = soil heat flux, u_{2m} = wind speed measured two meters above the surface of the ground. The FAO approach takes the various crop conditions into account thanks to the k_{crop} coefficient that transforms the potential evaporation of the reference surface (in square brackets) into PE in relation to the actual surface (a bare surface in the case at hand). This coefficient was quantified in Rianna et al., (2014) as $k_{crop} = 1.15$ by using PE measurements provided by the physical model. It proves consistent with literature indications (Allen et al., 1998; Allen et al., 2005).

It is important to highlight that the model described above incorporates evaporation as both a superficial and an internal phenomenon, suited to reproducing the possible deepening of the water state-change surface over dry hot periods. Hereafter, this model will be referred to as the "Internal Evaporation Model" or "IEM."

A simplified version of the described model particularizes into the Richards equation. It consists of the water balance equation (1) for liquid water, thus removing the vapor flow term, and equation (4), specified by equation (5) and (6). This isothermal approach only takes into account changes in atmosphere temperature through eq. (5), where it is assumed that $T_s = T_a$ (an approach called "isothermal model with atmospheric coupling", by Fredlund et al., 2012). The model takes only evaporation into account as a boundary phenomenon, which occurs only at the top-boundary, with no possibility of a downward shift of the water state-change surface. Hereafter, this model will be referred to as the "Boundary Evaporation Model" or "BEM".

A further simplification often adopted in single applications (Pagano et al., 2010) or in a number of codes developed to estimate slope stability conditions over extensive sloping territory (Iverson, 2000; Montgomery and Dietrich, 1994; Baum et al., 1998) corresponds to the latter (Richards equations) approach applied without accounting for evaporation. This model will subsequently be referred to as the "No Evaporation Model" or "NEM".

2.4 Calibration and model parameters

The IEM model is a generalization of the other two, implying that the soil properties and parameters it contains also pertain to BEM and NEM. Calibration refers to both thermal (soil thermal conductivity and volumetric specific heat) and hydraulic properties (the soil water retention curve and the hydraulic conductivity function), the latter being common to the other two approaches.

Parameters were calibrated from the results provided by the physical model over the first two years. The results collected over the subsequent two years were adopted to validate the calibration. Some of the soil properties were quantified directly from measurements. This is the case of the water retention function, which was obtained as best fit function of (water content) – (suction) points recorded at all depths by TDRs and jetfill tensiometers (Fig. 9a). This is also the case of the thermal conductivity function (λ), which was derived as best-fit function (Fig. 9b) of (water content) – (thermal conductivity) points

recorded at all depths. Thermal conductivity values were obtained using heat dissipation probes, referring to the relationship relating probe energization q, to q-induced temperature changes ΔT (Shiozawa and Campbell, 1990):

$$q = 4\pi \ln(\Delta T)\, \lambda \tag{7}$$

which contains λ as a single unknown.

The volumetric specific heat C_h and hydraulic conductivity functions, on the other hand, were quantified following articulated experimental data interpretation procedures based on back-analysis works.

C_h was determined by solving the heat equation at sublayers with the thicknesses demarcated by triples of temperature measurement points. By assuming that the energy spent for evaporation within each sublayer is negligible, and λ is constant at the mean value assumed throughout the sublayer ($\bar{\lambda}$), the heat equation may be rewritten as:

$$\frac{\partial T}{\partial t} = \frac{\bar{\lambda}}{C_h}\frac{\partial^2 T}{\partial z^2} \tag{8}$$

This equation was solved by regarding the two external temperature measurements of the sublayer as boundary conditions and considering internal measurement T^*, a reference for calibrating $\bar{\lambda}/C_h$, as the value that gives the best fit of the evolution of T^* over the first two years of observations. Preliminary knowledge of $\bar{\lambda}$ then makes it possible to obtain C_h (Fig. 10).

Having established all the parameters except the hydraulic conductivity function, the remaining parameter was calibrated via a back-analysis of the hydrological behaviour of the layer observed over the first two years. A domain of the same thickness (0.75m) as the layer placed in the physical model was assumed to be subject to boundary conditions at the top surface reproducing the recorded atmospheric variables. Figure 11 shows that the agreement between measurements and predictions obtained from the back-analysis is satisfactory both in terms of water storage (Fig. 11a) and suction (Fig. 11b). Predictions match observations not only within the calibration range but also outside it (validation phase). Figure 12 plots the hydraulic conductivity function resulting from back analysis. The hydraulic conductivity of the material drops by three orders of magnitude (from 10^{-6} to 10^{-9} m/s), with suction increasing from 0 to 100 kPa.

Upon completion of parameter calibration, thermal functions λ and C_h were further validated by checking their ability to reproduce the observed thermal behavior under the effects of the recorded atmospheric variables. Figure 13 shows that the model yields temperature predictions fully consistent with temperature measurements at all depths over the four years of available observations.

As stated previously, IEM calibration also implies automatic BEM and NEM calibration. Figures 14a and 14b add the predictions yielded by the BEM model in terms of WS and suction to the plots of Figure 10. It may be observed that even the approach incorporating evaporation as only a boundary phenomenon performs well in reproducing the recorded hydrological pattern. The predictions yielded by the two approaches (IEM and BEM) match during winter and early spring, in the meanwhile

that actual evaporation attains potential levels, and evaporation really configures as a boundary phenomenon. They depart instead during late spring, summer and autumn, when internal evaporation phenomena take place, or the effects of their previous occurrence are felt. During these periods, IEM predictions reproduce observations better than BEM ones, as the latter overestimates (or underestimates) water storage (suction).

3 Results and discussion

3.1 Patterns of AE predictions under simplified PE evolutions

In order to further investigate differences in the predictions yielded by the IEM and BEM models and their possible implications for the prediction of the evolution of the hydrological state, the model responses were compared under much simpler boundary conditions than those (Fig. 14) considered in reproducing the behaviour of the physical model. With the models calibrated as described above, the two approaches incorporating evaporation were used to predict actual evaporation fluxes (AE) they return under the effects of the same virtual potential evaporation (PE) flux applied at the top boundary, acting with an intensity of 4.5 mm per day and maintained constant over 60 days. The response of the two models was plotted in terms of both AE evolution (Fig. 15a) and hydraulic conductivity evolution at the top surface (Fig. 15b). The AE values yielded by the two models coincide when AE is equal to PE, in line with what was illustrated above in discussing the trends in Figure 14. There is a time, under such forcing, when AE departs from PE in the two predictions. It corresponds to the moment when upward water fluxes are no longer able to fully supply the top surface with that water amount satisfying the hypothesized atmospheric demand for evaporation (4.5 mm per day). After this time, the two AE predictions also diverge and follow a substantially different evolution. A drop in AE typifies the BEM model response. This is due to the fact that the model generates vapor only from liquid water reaching the top surface. When AE diverges from PE, a shallow thin zone placed below the top surface desaturates more than the interior. With increasing suction, hydraulic conductivity decreases and hydraulic gradients increase, with the former having a greater effect on flow reduction (Fig. 15b). In turn, this reduction slows the upward water flux, so that that water losses induced by the PE action in this shallow thin zone are no longer compensated by water supplied from the interior. In this way, the desaturation process goes on up to shortly lead the shallow-thin zone to the residual water content and at a very low hydraulic conductivity. At this point, the upward water flux from the interior is almost totally inhibited, in a sort of barrier effect exerted by the shallow thin zone, implying the vanishing of AE. This barrier effect inhibits further desaturation processes inside the domain. Consistently, suction attains very high values within the cap zone, remaining at low levels inside the domain.

On the other hand, the IEM model is suited to reproduce the occurrence of internal evaporation as soon as the zone placed below the top surface desaturates more than the interior at the time of PE-AE divergence. Vapor starts to generate within the interior of the domain other than at the boundary, in an automatic and progressive deepening of the water phase-change surface. Interior vapor forms and migrates upward at a rate that is now regulated by vapor conductivity, which unlike with hydraulic

conductivity, progressively increases as the degree of saturation decreases so that vapor migration takes place at a rate that maintains AE at significant levels. It follows that AE reduction is gradual in the IEM predictions as it is effectively supplied by the interior vapor generation. Furthermore, as internal vapor approaches the top-surface, it also reduces suction levels there as a consequence of thermodynamic equilibrium (Eq. 3). This contributes to maintaining hydraulic conductivity at levels much higher than those associated with the BEM prediction. Boundary evaporation also occurs at a consistently higher rate, or, in other words, the formation of any barrier effect is prevented. Compared with BEM prediction, in the IEM prediction, vapor migration produces suction levels (Fig. 15c) that are lower near the top surface and higher within the domain interior when desaturation processes are more significant.

3.2 Interpretative analyses of the Nocera Inferiore 2005 landslide

In order to investigate the potential of the IEM and BEM models in interpreting the Nocera Inferiore 2005 case history and establishing their reliability as predictive tools in early warning systems, a two-meter thick domain corresponding to the thickness of the cover in the zone where the landslide triggered was analysed. The analyses were carried out according to the hypotheses formulated in section 2.3, quantifying the model parameters as described in section 2.4 describing calibration procedures. The evolution of meteorological variables recorded at the landslide site over the whole ten years (Fig. 3), including the time of the landslide, was converted into the evolution of the hydrological state of the domain via the IEM and BEM predictions. The hydrological state was assessed in terms of water storage (WS) and suction in the middle of the domain analysed (to a depth of 1 m). In possibly using these models for physically based early predictions, these variables, being strictly related to slope safety conditions, may be adopted as proxies from which different alert thresholds can be defined.

Figure 16 plots the WS evolutions yielded by IEM and BEM analyses. Both are able to reproduce the typical WS patterns that develop over a hydrological year, so as shown by the experimental data provided by the physical model: WS fluctuates during the year, increasing during autumn, winter and early spring due to precipitation, and reducing during late spring and summer due to evaporation.

The IEM and BEM trends differ systematically during the dry seasons as a result of the different AE mechanisms that activate as soon as significant drying processes cause AE to diverge from PE (see §3.1). The minimum WS values predicted by the two models during the dry periods are different, as already observed in the results meant to fit the data for the physical model (Fig. 14a). However, differences in minimum values are now higher than those previously computed, essentially due to the different domain thicknesses analysed (2 m instead 0.75 m). The 0.75 m domain is so small that the meteorological forcing typical of the dry periods produces water content to attain residual value throughout the whole thickness. Most of the drying processes (WS reductions) are regulated by AE=PE. Only a residual part of the WS (from the point of departure down to the minimum) occurs because of internal evaporation. Under these conditions, IEM and BEM effectively work in a similar way most of the time, producing a small gap at the lowest WS. A 2-meter thick domain, under the effects of similar meteorological forcing, does not achieve residual water content at all depths during the dry season. WS losses regulated by internal evaporation

are far from minor and represent a significant part of the evaporated water, so that a significant gap is present at the lowest WS. This is of around 150 mm for the years characterized by matching WS during the wet season.

WS gaps attained during the dry season are reflected in WS differences during the subsequent wet season (autumn), when landslide susceptibility is usually moderate. These differences tend to be gradually attenuated with the passing of time due to the higher potential infiltration in the IEM domain caused precisely by its drier state: the WS trend yielded by IEM is marked by higher hydraulic gradients. In some seasons, IEM predictions always remain below those of the BEM, while in others the WS gaps disappear. The occurrence of one or the other condition depends essentially on rainfall cumulating over the autumn wet season. When the IEM prediction and the BEM match, AE=PE usually occurs, so that IEM and BEM predictions coincide over the entire subsequent wet period. This happened during the four consecutive hydrological years from September 2002 to the August 2006 landslide, including the landslide year.

A peak at record is yielded by both IEM and BEM analyses at the time of the landslide (Fig. 16a). By enlarging the scale and looking at high WS values in order to isolate and highlight peaks (Fig. 16b), it may be observed that the peaks attained at the time of the landslide are higher than the peaks attained over other years. This encourages the assumption that both predictions, as they clearly indicate a peculiarity in the hydrological response in the cover at the time of the landslide, would have worked satisfactorily if they had been adopted as predictive tools in an early warning system. In fact, they would have been able to indicate a situation of alarm at the time of the landslide without generating a significant number of false alarms if the alarm threshold had been placed slightly below the peak attained at landslide time.

Figure 17 shows the IEM and BEM predictions for the evolution of suction at a depth of 1 m. It reveals that suction predicted also at the middle of the layer may work as a proxy for slope safety conditions, as the hydrological behavior it depicts is consistent with everything indicated by the integral variable WS. Suction or WS may therefore both be used as reference variables for early warning.

Figure 18 shows the water storage evolution yielded by the simplest model (NEM) adopted, which neglects evaporation entirely (Pagano et al., 2010; Reder et al., 2017). In this case, it is not possible to carry out a continuous analysis of the hydrological response of the cover over the whole ten years, due to the inability of the model to predict water losses from the domain during the dry periods. Analysis needs to be restarted at the beginning of each hydrological year in order to reinitialize the hydraulic variables. Unfortunately, these become additional input data that have to be set. It would be necessary, in theory, to monitor suction or water content in the field to quantify initial conditions. The initial quantification of suction has a particular impact on the reliability of the analysis during the periods of landslide susceptibility occurring not far from the start time (considered at the beginning of the hydrological year), as the effects of the starting conditions are lost after a period of around four months (Pagano et al., 2010). In these predictions, suction re-initialization at the beginning of each hydrological year is achieved by adopting suction values yielded by the IEM model, as it is information obtained by monitoring suction in the field. The NEM prediction has a peak at the time of the landslide, once again at record levels both in terms of water storage and suction, but the peak is not as high as a large number of other significant peaks. From the point of view of performance, NEM by itself must therefore be considered less effective than the IEM and BEM predictions together.

The performances of the three adopted approaches may be judged by taking the number of alerts and alarms they would have yielded if they had been adopted as predictive tools in an early warning system within the specific reference period analysed. Differences in performance obviously depend on the levels at which the thresholds for water storage or suction are set to limit the different alert stages and spread the alarm. The alarm threshold can be identified by interpreting the landslide phenomenon by the models, referring to the prediction yielded by the most complete one (IEM) in terms of the lowest suction level not associated with a landslide (around 3.5kPa). A possible pre-alarm alert level is 5 kPa, obtained by increasing the alarm threshold by around 50%. This double choice permits a quantitative comparison of model performance, with the IEM model performing the best, returning 0 alarms and 1 alert (1 every 11 years). The BEM comes second, returning 3 false alarms (1 every 3.7 years) and 5 alerts (1 every 2.2 years). The NEM model performs worst, returning 5 false alarms (1 every 2.2 years) and 12 alerts (0.9 for year).

4 Conclusions

This paper has investigated the performance of three physically based models taken from the literature with a view to using them for early warning predictions. Two of them incorporate evaporative fluxes, but the other neglects them. Particular care has been taken with the simplification of the models so as to respect the accuracy of the predictions they provide, establishing procedures to calibrate the parameters and to characterize the hydrological patterns they predict. The models' performance has been assessed by using them to interpret the case history of a landslide and examine their ability to indicate any hydrological peculiarity at the time of the landslide.

With regard to calibrating the parameters, the study provides a quantification of the parameters suited to a material widespread in the Campania Region and, most probably, in other sites in the world. For these materials and similar, the quantification of the parameters is ready for use and should simplify the task of setting up an early warning system. The study provides calibration procedures for other types of materials, some of them specific, if lysimeter data are available; others are applicable also to data obtained from field monitoring.

Concerning performance, the study shows that all models, if used as early warning predictive tools, would then be able to signal the alarm at the time of a landslide. Increased complexity and completeness of the models, however, would clearly result in a lower number of false alarm predictions.

For the sake of simplicity and given the availability of monitored data relating to a physical model covered by a bare surface, this condition has been assumed for the purposes of calibration, validation and interpretation of case histories. Nevertheless, in natural slopes, the effect of transpiration from vegetation may well play a significant role. From this point of view, the availability of monitored data provided by the lysimeter for the hydrological years 2014-2017, during which the surface was constantly covered by natural vegetation would be worthy of further investigation.

References

Allen, R.G., Pereira, L.S., Raes, D., Smith, M., and Ab, W.: Crop evapotranspiration - Guidelines for computing crop water requirements, FAO Irrigation and Drainage Paper, 56; doi:10.1016/j.eja.2010.12.001, 1998.

Allen, R.G., Pruitt, W.O., Raes, D., Smith, M., and Pereira, L.S.: Estimating evaporation from bare soil and the crop coefficient for the initial period using common soils information, J. Irrig. Drain. Eng., 131, 1, 14–23, 2005.

Baum, R.L., Savage, W.Z., and Godt, J.W.: TRIGRS – A FORTRAN program for transient rainfall infiltration and grid-based regional slope stability analysis, vers. 2.0, U.S. Geol. Survey Open-File Rep. 2008-1159, 75pp, 2008.

Brand, E. W., Premchitt, J. and Phillipson, H. B. Relationship Between Rainfall and Landslides in Hong Kong, Proc. 4th Int. Symp. on Landslides, Toronto, Vol. 1, pp. 377-384, 1984

Chatterjea, K. Observations on the Fluvial and Slope Processes in Singapore and their Impact on the Urban Environment, PhD Thesis, National University of Singapore, 1989

de Riso, R., Budetta, P., Calcaterra, D., and Santo, A.: Riflessioni sul comportamento delle colate rapide non incanalate della Campania, alla luce delle conoscenze pregresse, Proceedings National Conference on "La Mitigazione del Rischio da Colate di Fango", Napoli, May, 2–3, 2005, 81-92, 2007

Formetta, G., Rago, V., Capparelli, G., Rigon, R., Muto, F. and Versace, P.: Integrated Physically based system for modeling landslide susceptibility, Procedia Earth Planet. Sci., 9, 74–82, doi:10.1016/j.proeps.2014.06.006, 2014.

Fredlund, D.G., Rahardjo, H., and Fredlund, M.D.: Unsaturated soil mechanics in engineering practice. John Wiley & Sons, Inc., Hoboken, New Jersey, 2012.

Geo-Slope: Vadose Zone Modeling with VADOSE/W 2007: An Engineering Methodology, Third Edition, Calgary, Alberta, Canada, 344 pp., 2008.

Iverson, R.M.: Landslide triggering by rain infiltration, Water Resour. Res., 36, 1897–1910, 2000.

Liao, Z., Hong, Y., Kirschbaum, D., Liu, C., Assessment of shallow landslides from Hurricane Mitch in Central America using a physically based model. Environ. Earth Sci. 66, 1697–1705. http://dx.doi.org/10.1007/s12665-011-0997-9, 2011.

Montgomery, D.R. and Dietrich, W.E.: A physically based model for the topographic control of shallow landsliding, Water Resour. Res., 30, 1153–1171, 1994.

Morgenstern, N. R. The Evaluation of Slope Stability A 25 Year Perspective, Proc. Stability and Performance of Slopes and Embankments II, Berkeley, California, Vol. 1, pp. 1-26, 1992.

Pagano, L, Picarelli, L., Rianna, G., and Urciuoli, G.: A simple numerical procedure for timely prediction of precipitation-induced landslides in unsaturated pyroclastic soils, Landslides, 7, 273–289, 2010.

Picarelli, L., Olivares, L., and Avolio, B.: Zoning for flowslide and debris flow in pyroclastic soils of Campania region based on infinite slope analysis, Eng. Geol., 102, 132–141, 2008.

Pirone, M., Papa, R., Nicotera, M.V., and Urciuoli, G.: In situ monitoring of the groundwater field in an unsaturated pyroclastic slope for slope stability evaluation, Landslides, 12, 259–276, 2015.

Reder, A., Pagano, L., Picarelli, L., and Rianna, G.: The role of the lowermost boundary conditions in the hydrological response of shallow sloping covers, Landslides, 14, 3, 861–873, doi:10.1007/s10346-016-0753-z, 2017.

Rianna, G., Pagano, L., and Urciuoli G.: Investigation of soil-atmosphere interaction in pyroclastic soils, J. Hydrol., 510, 480-492, 2014b.

Shiozawa, S. and Campbell G.S.: Soil thermal conductivity, Remote Sens. Rev., 5, 1, 301–310, 1990.

Rianna, G., Pagano, L., and Urciuoli, G.: Rainfall patterns triggering shallow flowslides in pyroclastic soils, Eng. Geol., 174, 22–35, 2014a.

Richards, L.A: Capillary conduction of liquids through porous mediums, J. Appl. Phys., 1, 318–333, 1931.

Teixeira, M., Bateira, C., Marques, F. and Vieira, B.: Physically based shallow translational landslide susceptibility analysis in Tibo catchment , NW of Portugal, Landslides, 12, 455–468, doi:10.1007/s10346-014-0494-9, 2015.

Tetens, O.: Uber einige meteorologische begriffe, Z. Geophys., 297–309, 1930.

Wilson, G.W., Fredlund D.G., and Barbour S.L.: Coupled soil–atmosphere modeling for soil evaporation. Can. Geotech. J., 31, 151–161, 1994.

Wilson, G.W., Fredlund, D.G., and Barbour, S.L.: The effect of soil suction on evaporative fluxes from soil surfaces, Can. Geotech. J., 34, 145–155, doi: 10.1139/t98-034, 1997.

Nat. Hazards Earth Syst. Sci. Discuss., https://doi.org/10.5194/nhess-2017-285
Manuscript under review for journal Nat. Hazards Earth Syst. Sci.
Discussion started: 7 September 2017

Natural Hazards and Earth System Sciences
Discussions

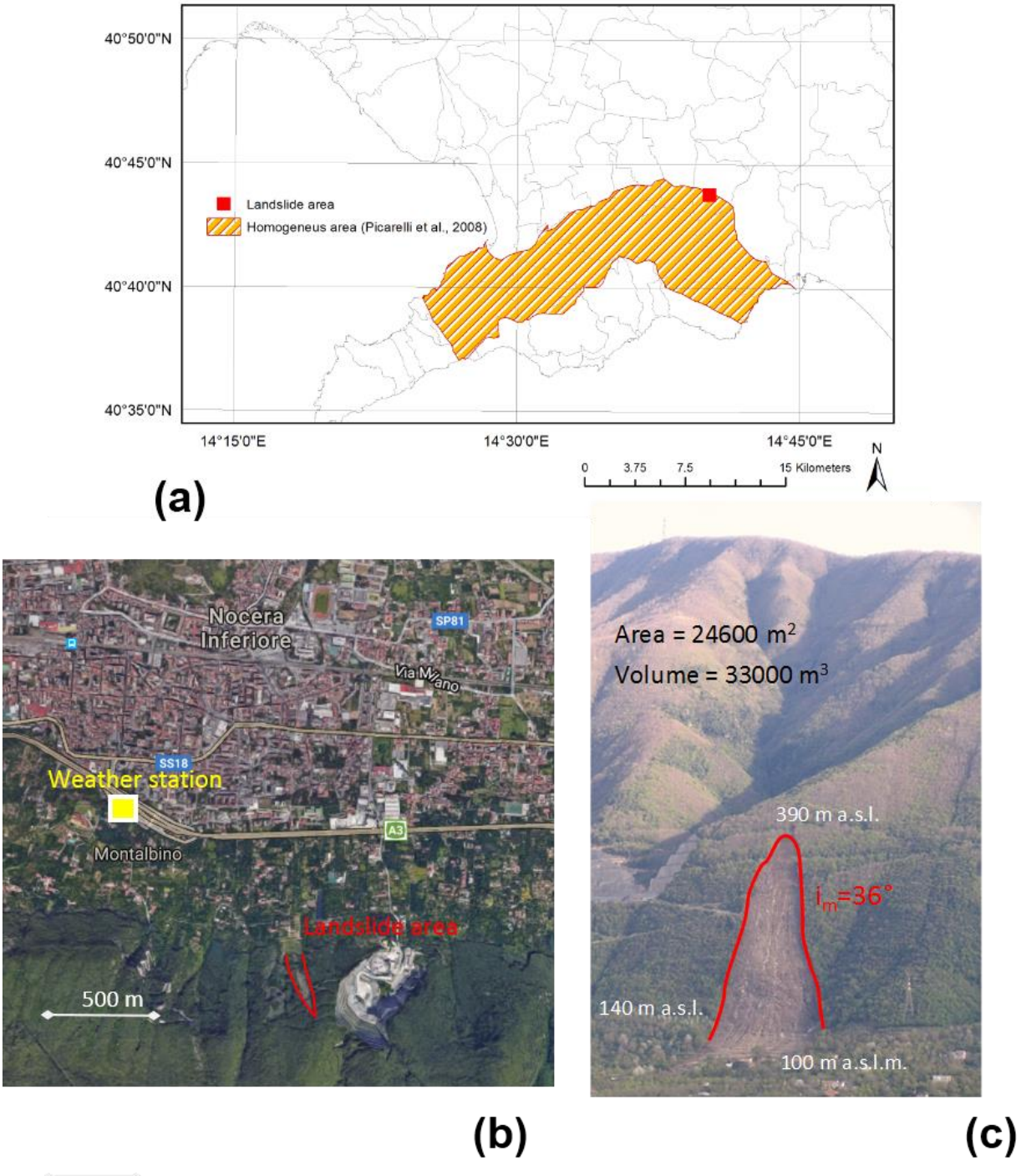

Figure 1: The 2005 Nocera Inferiore Landslide (2005NIL): (a) map indicating the landslide location and zones homogeneous with that of the landslide for soils, cover thicknesses and slope gradients; (b) plan view (DigitalGlobe 2012. http://www.earth.google.com), indicating the landslide area and the location of the weather station; (c) frontal view of the landslide area. (Pagano et al., 2010, modified).

Nat. Hazards Earth Syst. Sci. Discuss., https://doi.org/10.5194/nhess-2017-285
Manuscript under review for journal Nat. Hazards Earth Syst. Sci.
Discussion started: 7 September 2017

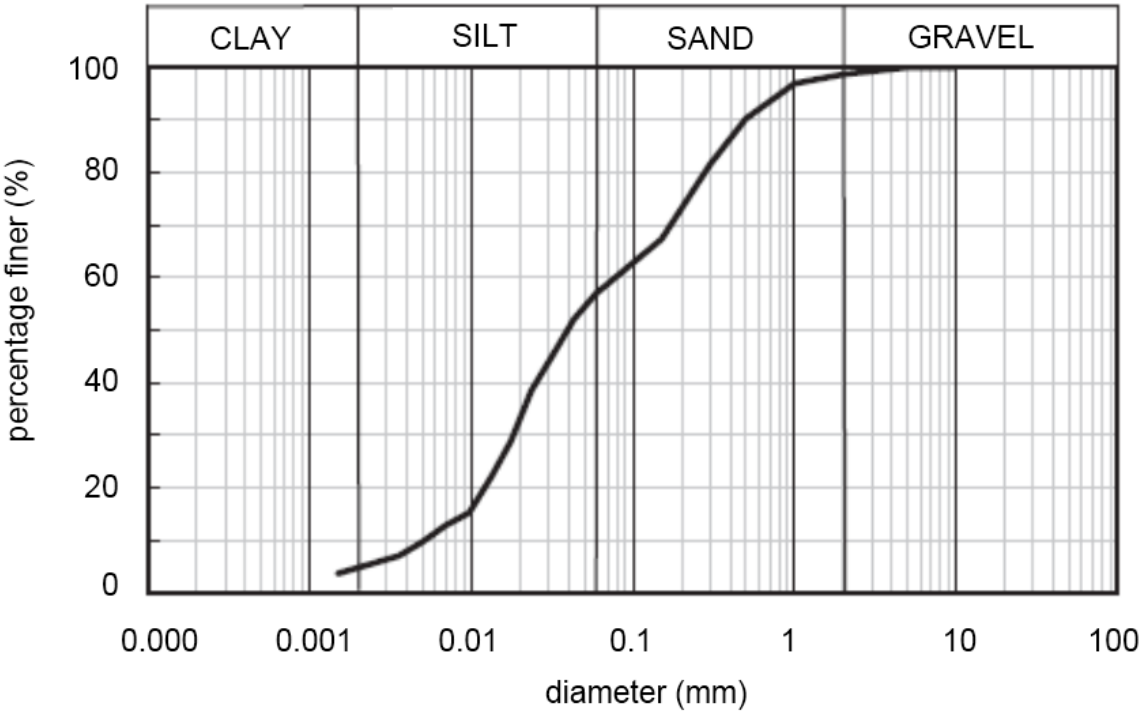

Figure 2: Grain-size distribution of the Nocera Inferiore volcanic ash (Pagano et al., 2010)

Nat. Hazards Earth Syst. Sci. Discuss., https://doi.org/10.5194/nhess-2017-285
Manuscript under review for journal Nat. Hazards Earth Syst. Sci.
Discussion started: 7 September 2017

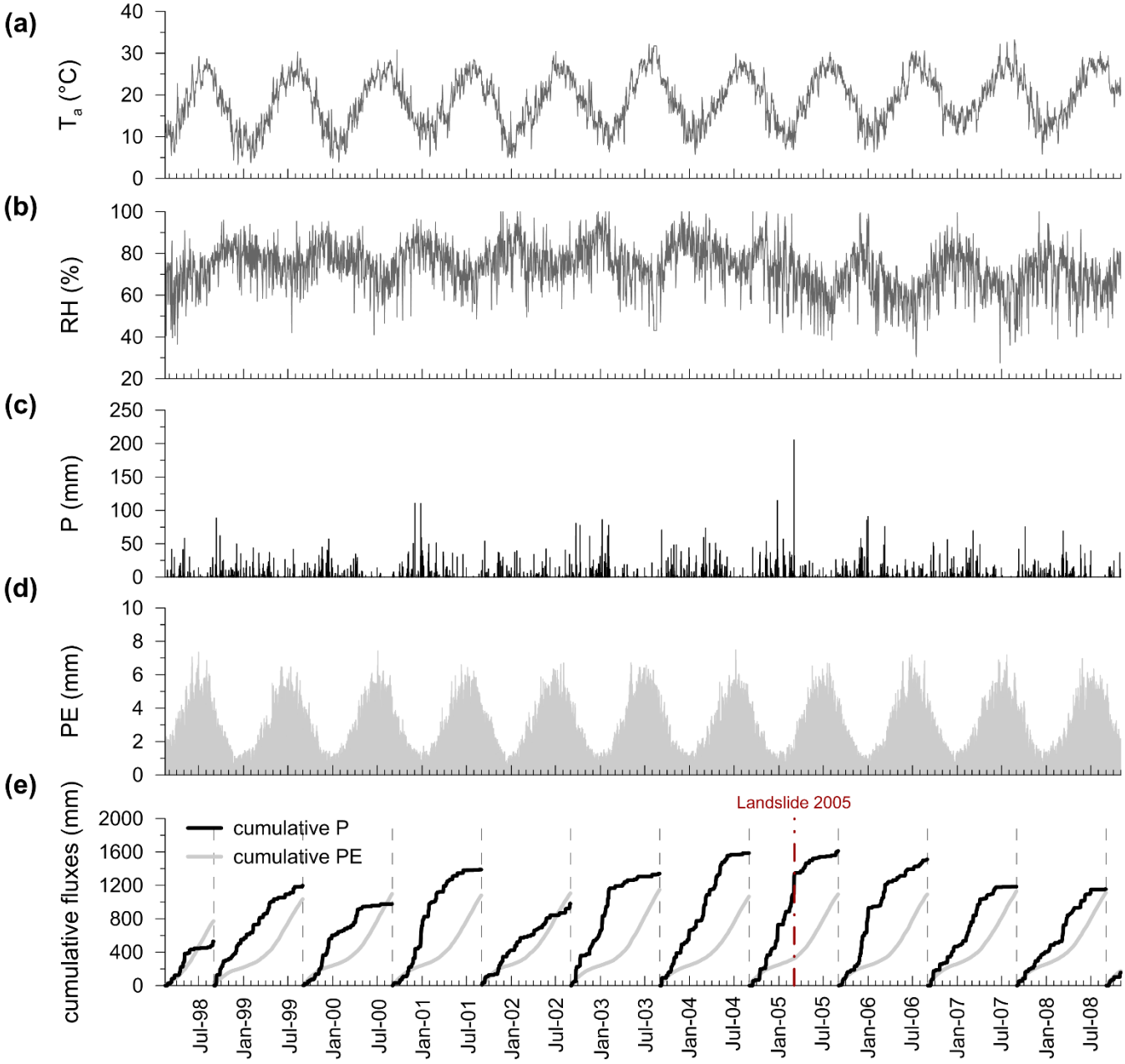

Figure 3: Meteorological variables recorded at the 2005NIL site between January 1998 and August 2008: (a) mean daily air temperature, T_a; (b) mean daily air relative humidity, RH; (c) daily precipitations, P; (d) daily potential evaporation, PE; precipitation, P, and potential evaporation PE, cumulated during each hydrological year

Nat. Hazards Earth Syst. Sci. Discuss., https://doi.org/10.5194/nhess-2017-285
Manuscript under review for journal Nat. Hazards Earth Syst. Sci.
Discussion started: 7 September 2017

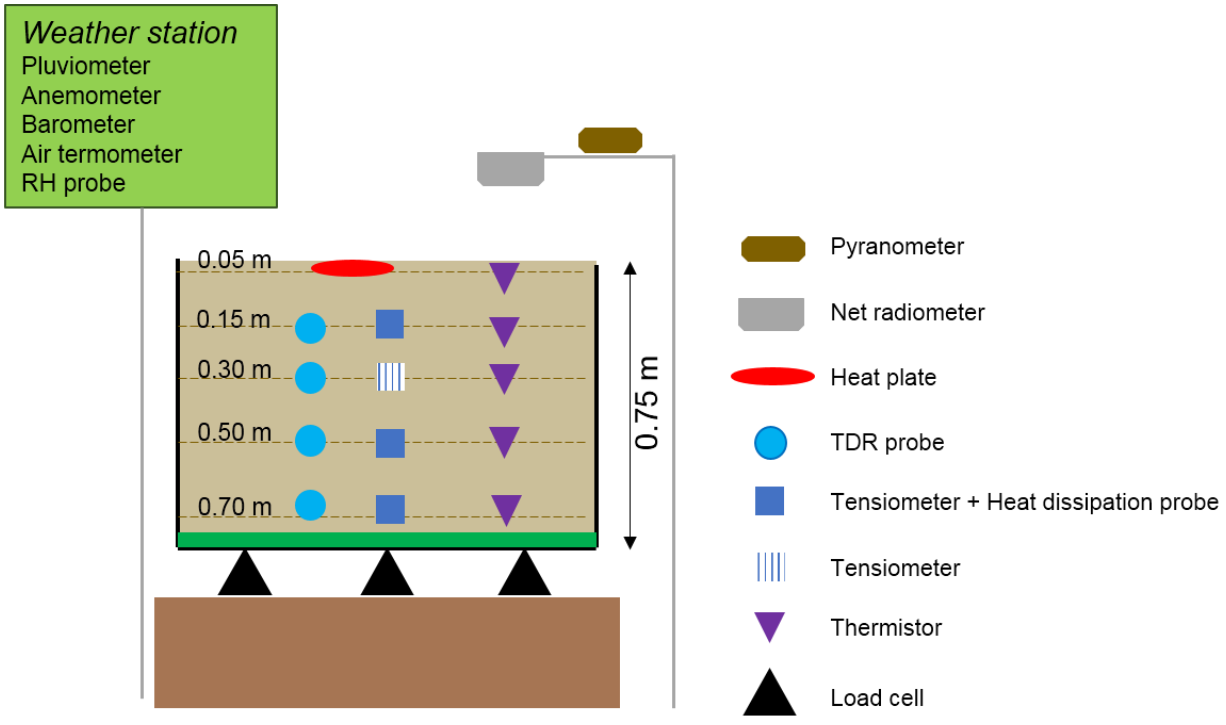

Fig. 4

Figure 4: Monitoring devices installed in the physical model (Rianna et al., 2014a, modified).

Nat. Hazards Earth Syst. Sci. Discuss., https://doi.org/10.5194/nhess-2017-285
Manuscript under review for journal Nat. Hazards Earth Syst. Sci.
Discussion started: 7 September 2017

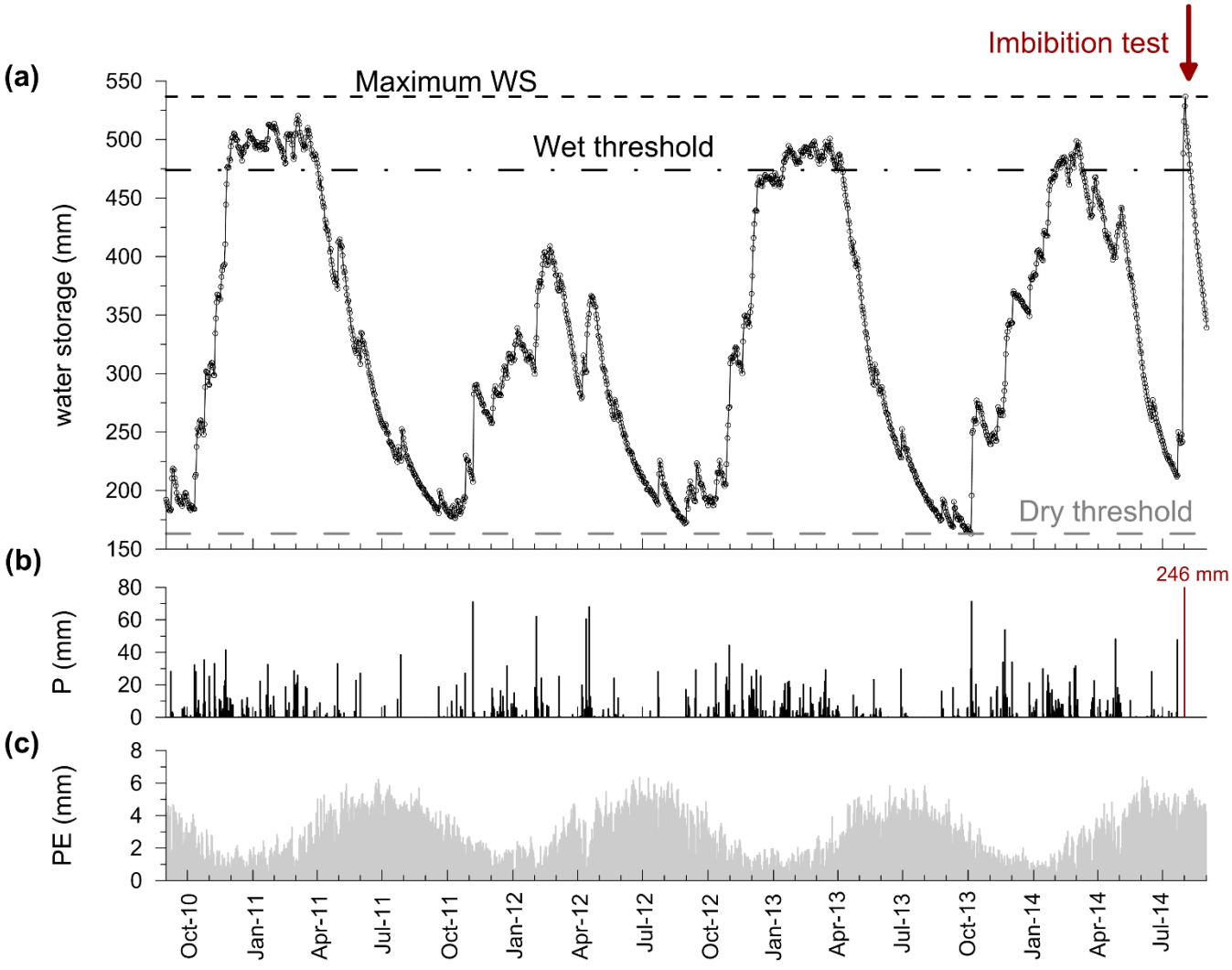

Figure 5: Evolution of variables recorded by the physical model of lysimeter: (a) layer water storage, WS; (b) daily precipitations, P; (c) daily potential evaporation, PE. (Records taken over the first two hydrological years are from Rianna et al., 2014a).

Nat. Hazards Earth Syst. Sci. Discuss., https://doi.org/10.5194/nhess-2017-285
Manuscript under review for journal Nat. Hazards Earth Syst. Sci.
Discussion started: 7 September 2017

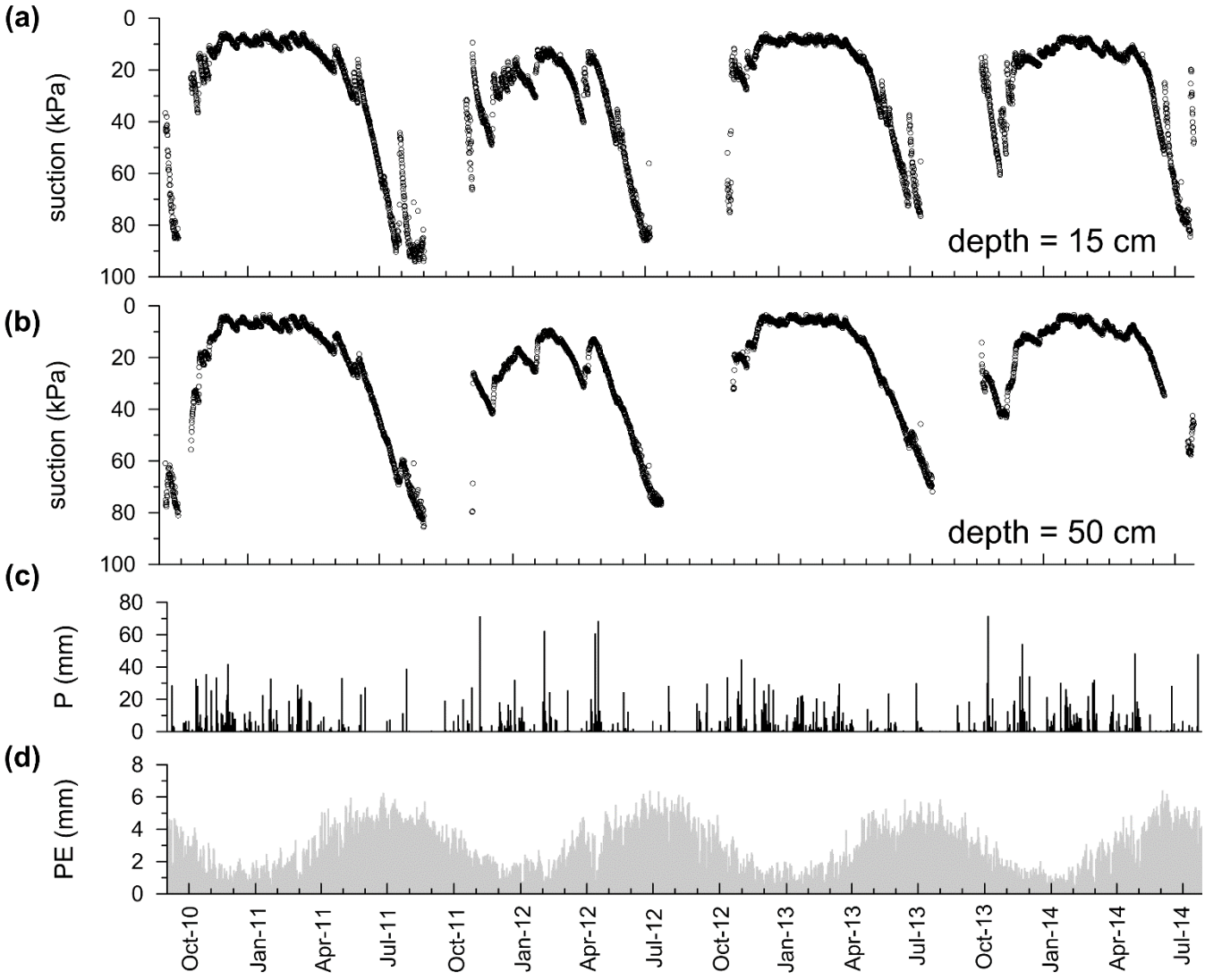

Figure 6: Evolution of variables recorded by the physical model of lysimeter: (a) matric suction at depth=15 cm; (b) matric suction at depth=50 cm; (c) daily precipitations, P; (d) daily potential evaporation, PE. (Over the first two hydrological years records are from Rianna et al., 2014a)

Nat. Hazards Earth Syst. Sci. Discuss., https://doi.org/10.5194/nhess-2017-285
Manuscript under review for journal Nat. Hazards Earth Syst. Sci.
Discussion started: 7 September 2017

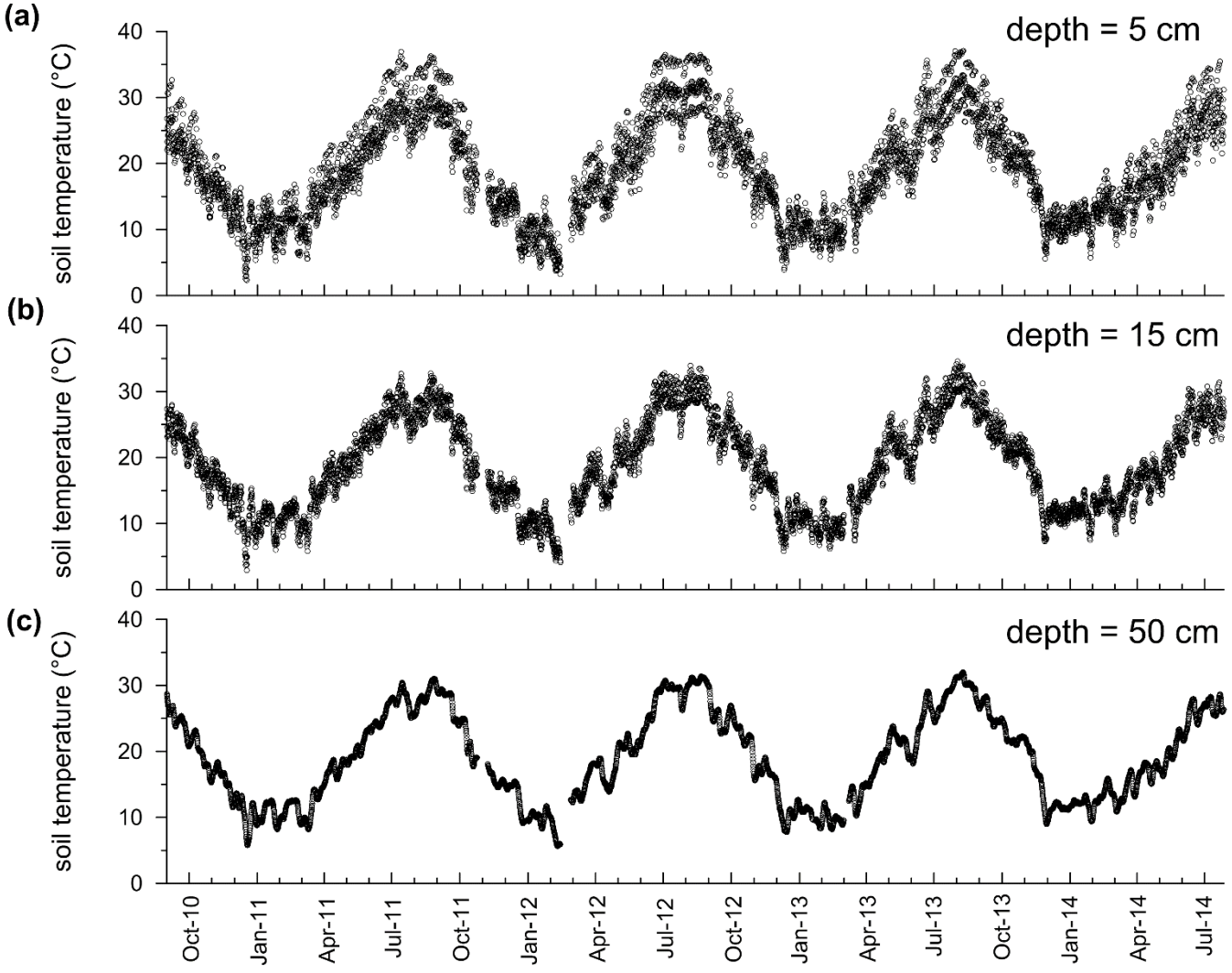

Figure 7: Evolution of temperature, T, recorded by the physical model of lysimeter: (a) soil temperature at depth=5 cm; (b) soil temperature at depth=15 cm; (c) soil temperature at depth=50 cm.

Nat. Hazards Earth Syst. Sci. Discuss., https://doi.org/10.5194/nhess-2017-285
Manuscript under review for journal Nat. Hazards Earth Syst. Sci.
Discussion started: 7 September 2017

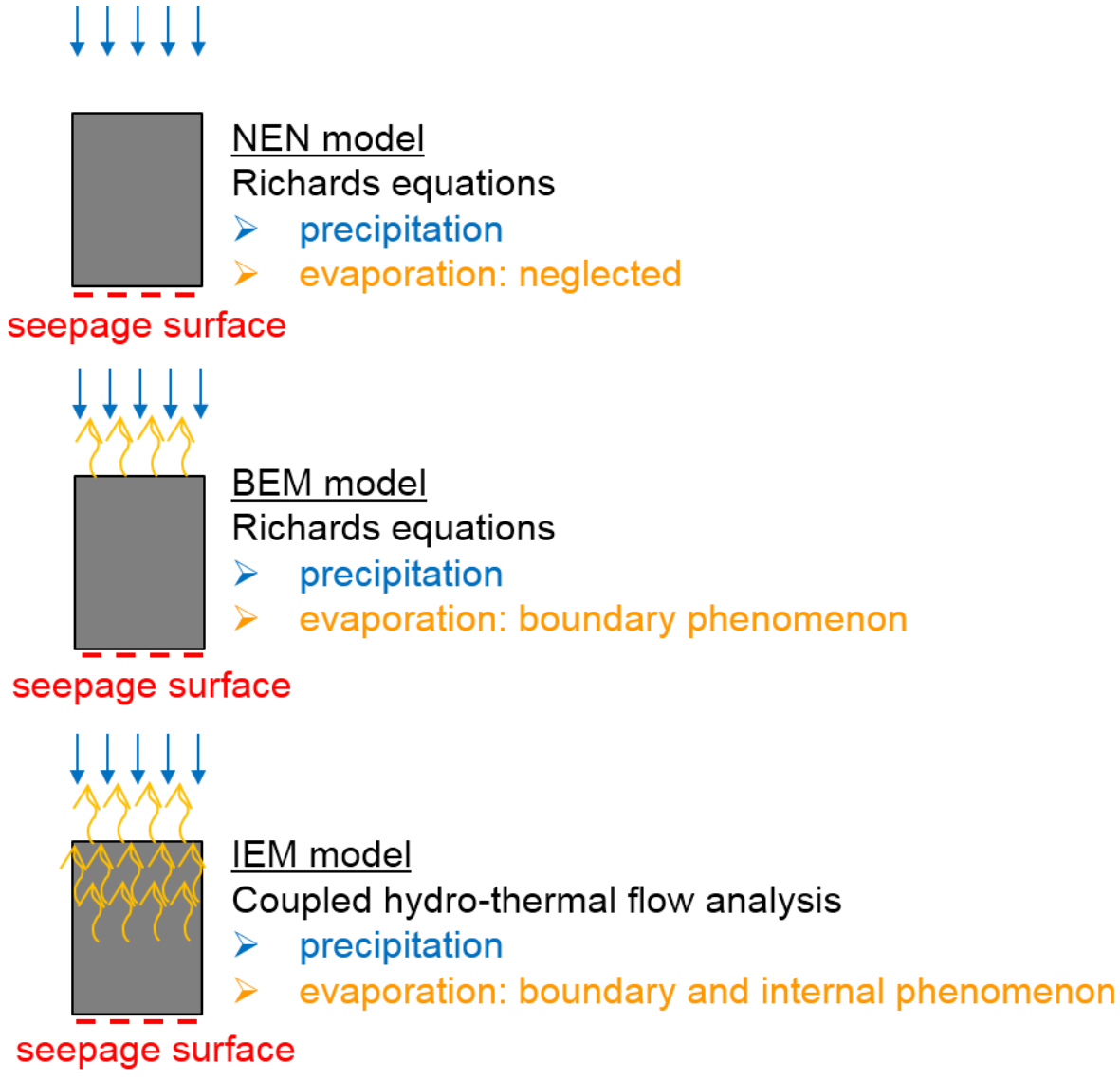

Figure 8: Model schemes adopted for early warning predictions.

Nat. Hazards Earth Syst. Sci. Discuss., https://doi.org/10.5194/nhess-2017-285
Manuscript under review for journal Nat. Hazards Earth Syst. Sci.
Discussion started: 7 September 2017

Natural Hazards and Earth System Sciences
Discussions

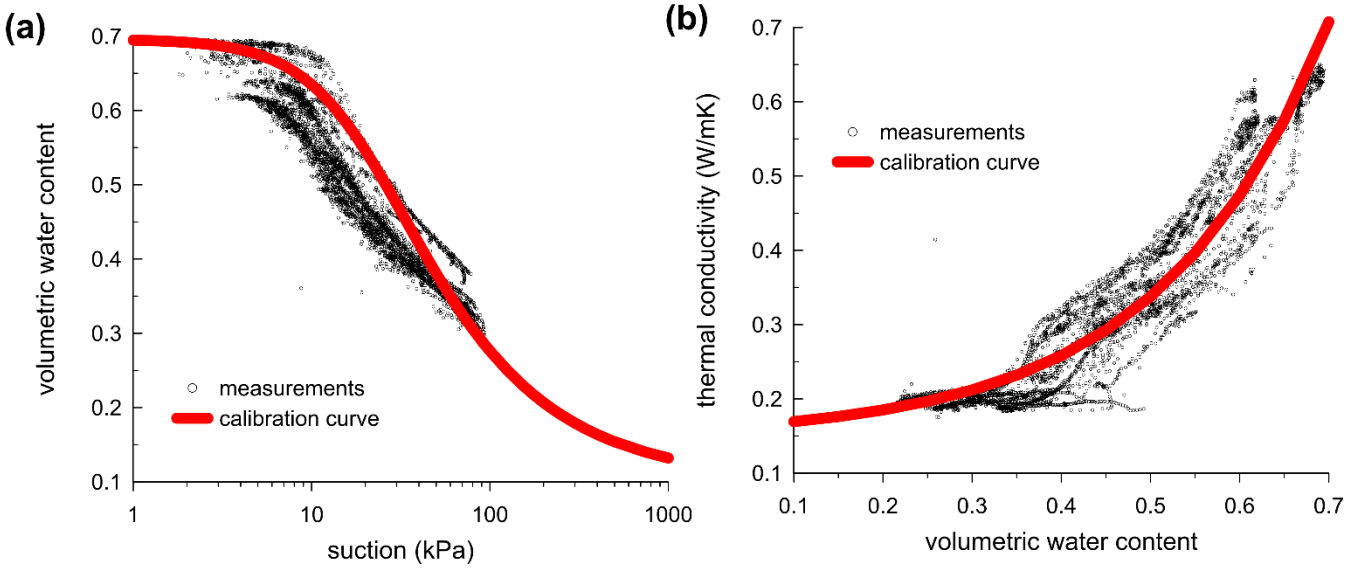

Figure 9: Calibration of model parameters: (a) experimental point versus fitting water retention curve; (b) experimental point versus fitting thermal conductivity function.

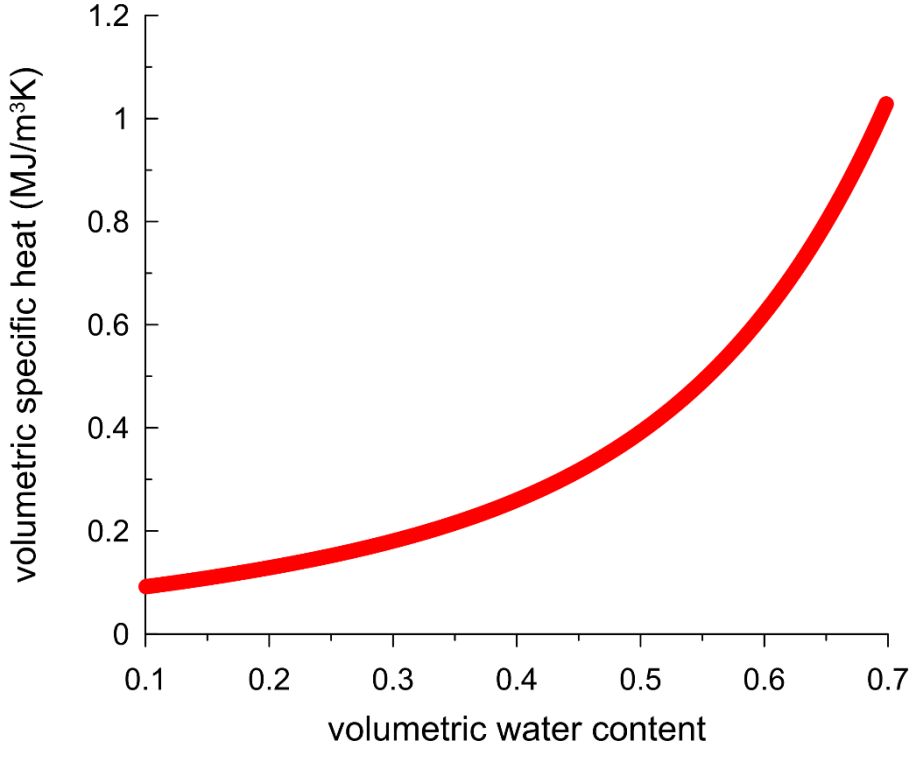

Figure 10: Calibration of model parameters: volumetric specific heat function.

Nat. Hazards Earth Syst. Sci. Discuss., https://doi.org/10.5194/nhess-2017-285
Manuscript under review for journal Nat. Hazards Earth Syst. Sci.
Discussion started: 7 September 2017

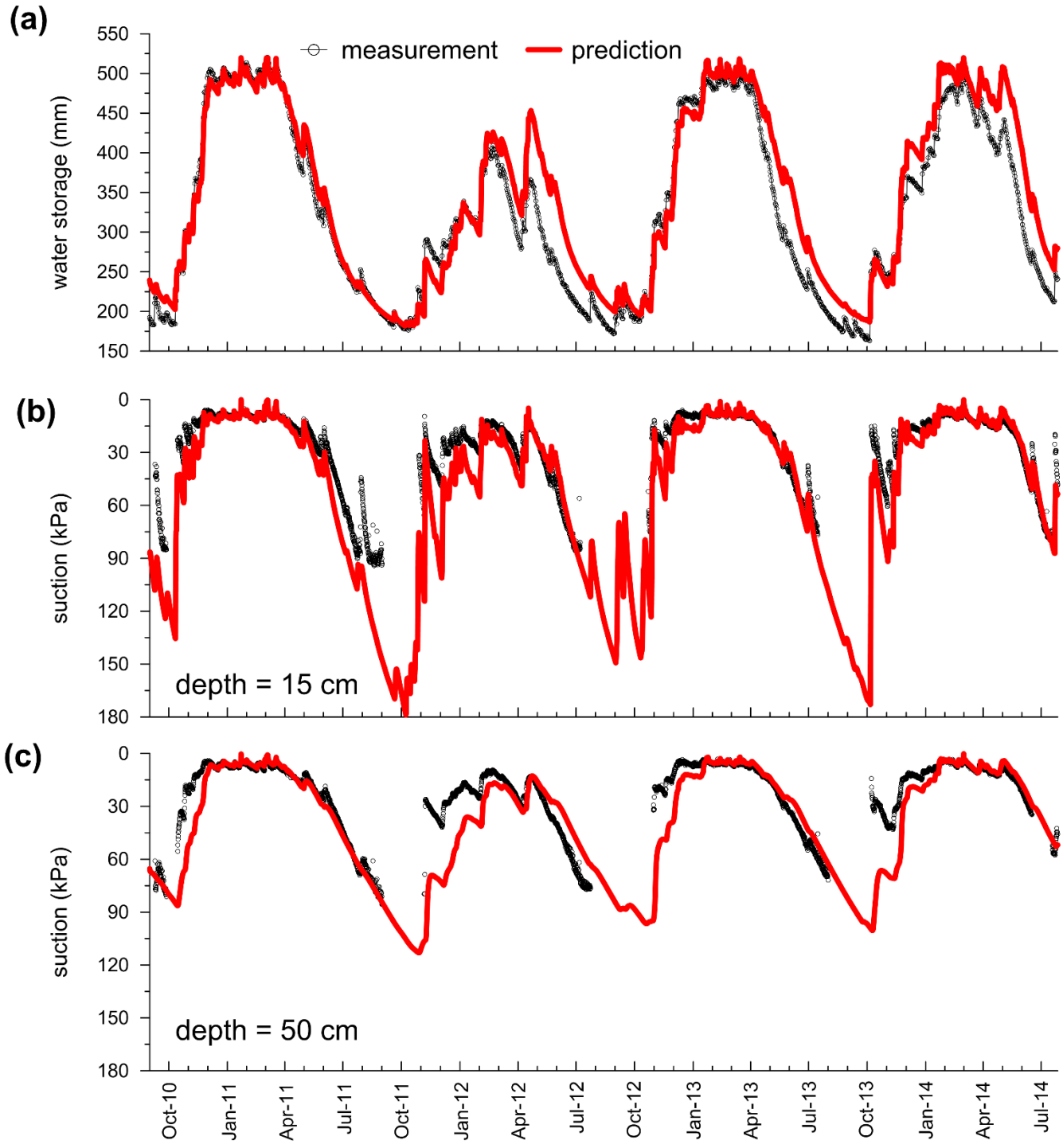

Figure 11: Back-analysis of the observed layer hydrological behavior by the IEM model: (a) measured versus IEM-predicted water storage, WS; (b) measured versus IEM-predicted suction at depth=15cm; (c) measured versus IEM-predicted suction at depth=50cm.

Nat. Hazards Earth Syst. Sci. Discuss., https://doi.org/10.5194/nhess-2017-285
Manuscript under review for journal Nat. Hazards Earth Syst. Sci.
Discussion started: 7 September 2017

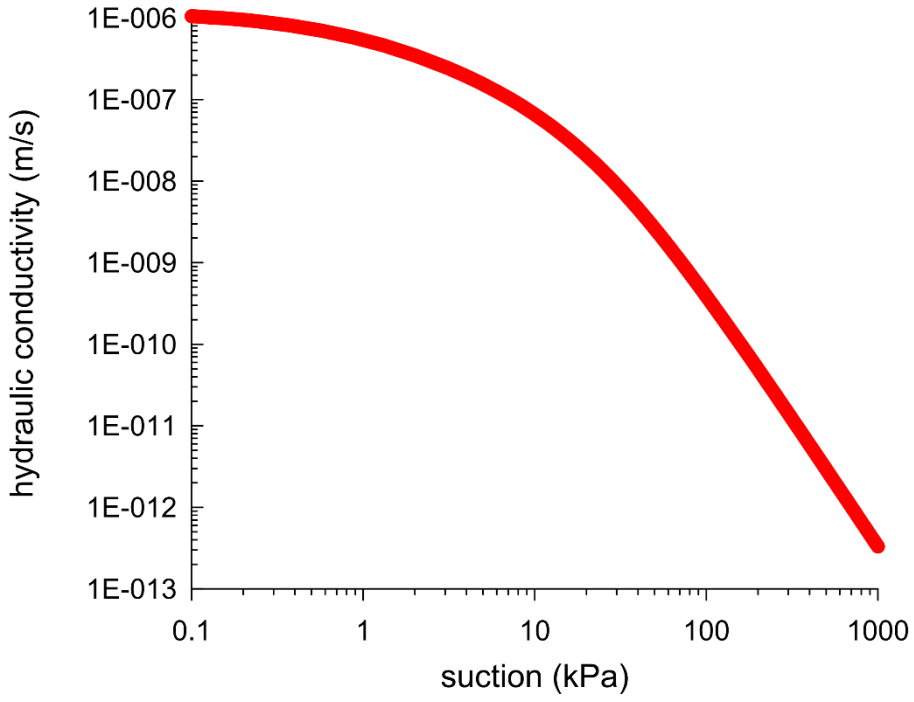

Figure 12: The hydraulic conductivity function obtained from the IEM-back-analysis of the hydrological behaviour.

Nat. Hazards Earth Syst. Sci. Discuss., https://doi.org/10.5194/nhess-2017-285
Manuscript under review for journal Nat. Hazards Earth Syst. Sci.
Discussion started: 7 September 2017

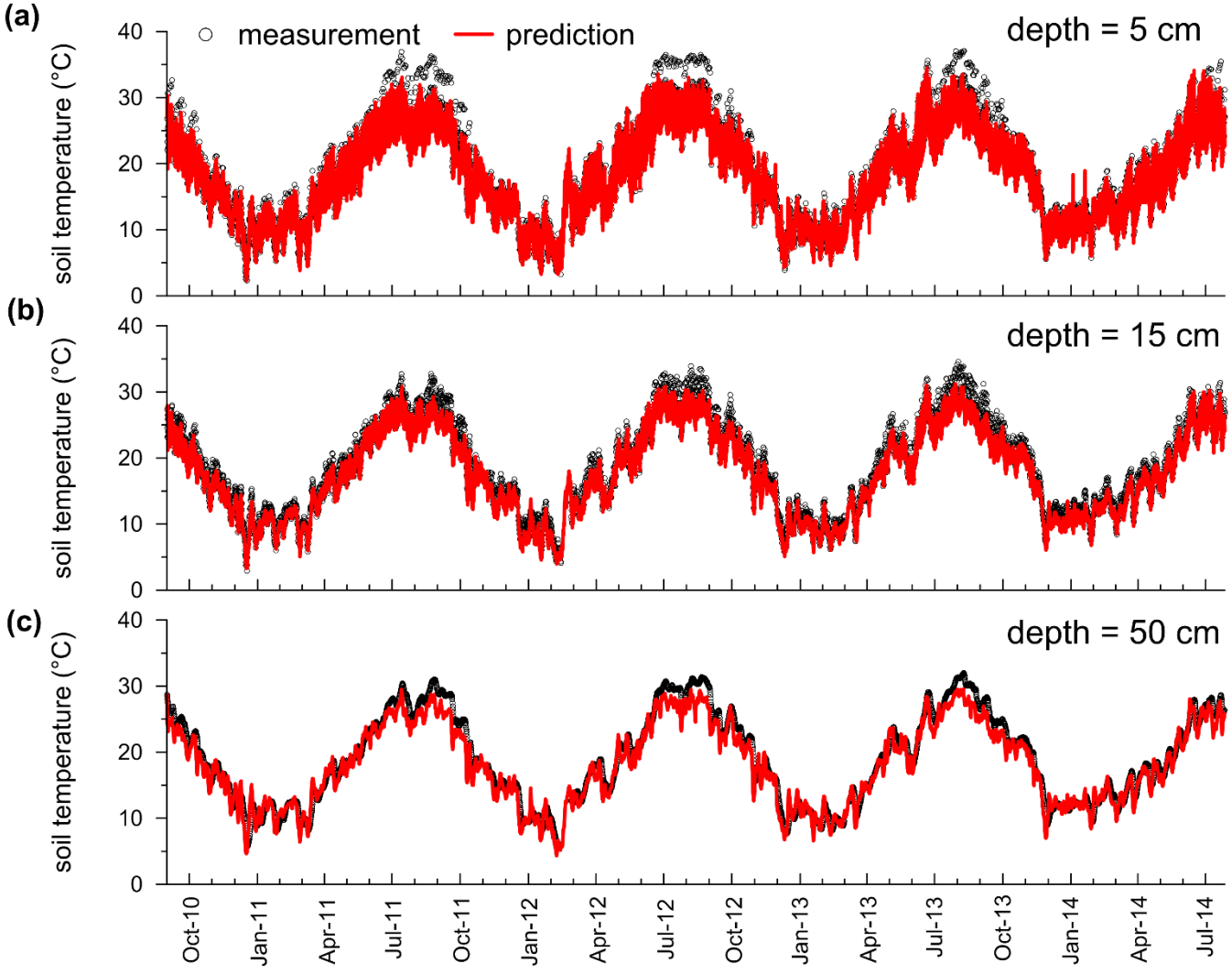

Figure 13: Measured versus IEM-predicted temperature (T) evolutions at three different depths indicated.

Nat. Hazards Earth Syst. Sci. Discuss., https://doi.org/10.5194/nhess-2017-285
Manuscript under review for journal Nat. Hazards Earth Syst. Sci.
Discussion started: 7 September 2017

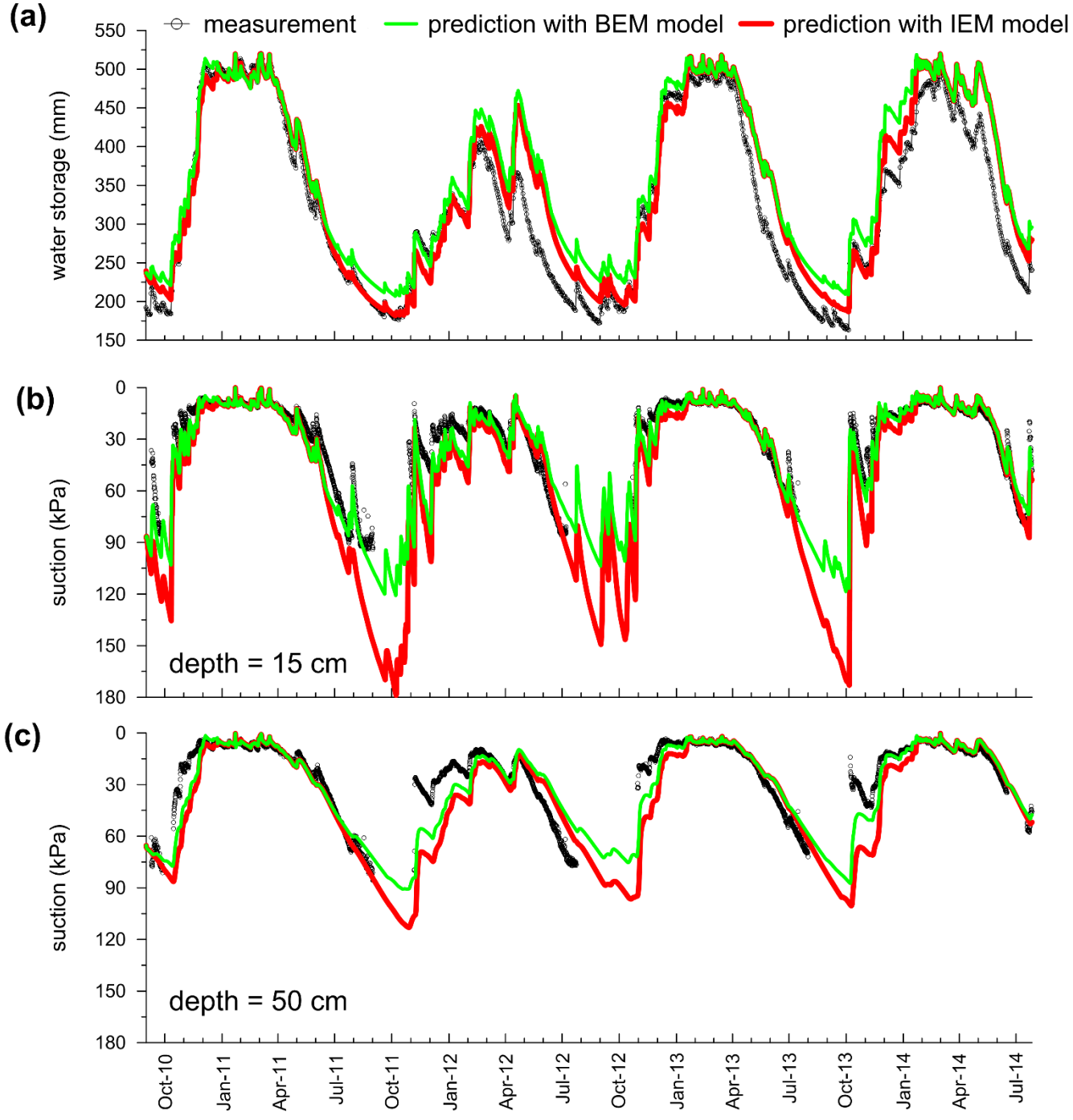

Figure 14: Comparison between IEM-predicted, BEM-predicted and observed hydrological behaviour: (a) comparisons in terms of water storage, WS, evolutions; (b) comparisons in terms of suction evolutions at depth=15cm; (b) comparisons in terms of suction evolutions at depth=50cm.

Nat. Hazards Earth Syst. Sci. Discuss., https://doi.org/10.5194/nhess-2017-285
Manuscript under review for journal Nat. Hazards Earth Syst. Sci.
Discussion started: 7 September 2017

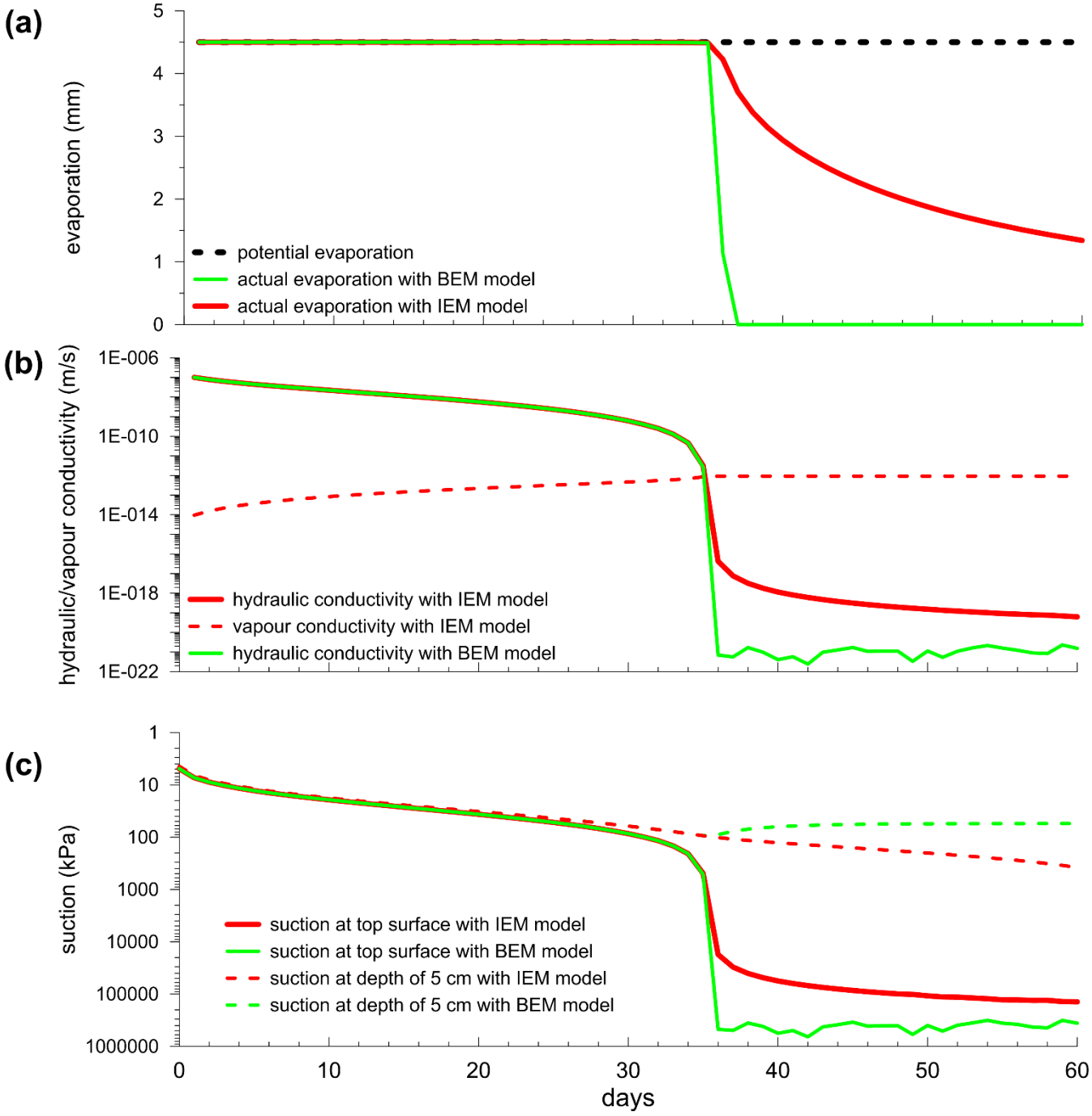

Figure 15: Comparison of variables yielded by IEM and BEM predictions under PE=4.5 mm/day: (a) comparisons between actual evaporation fluxes, AE; (b) comparisons between hydraulic conductivities at the top-surface and evolution of vapor conductivity at the top-surface; (c) comparisons between evolutions of suction at the top surface and at depth=5cm.

Nat. Hazards Earth Syst. Sci. Discuss., https://doi.org/10.5194/nhess-2017-285
Manuscript under review for journal Nat. Hazards Earth Syst. Sci.
Discussion started: 7 September 2017

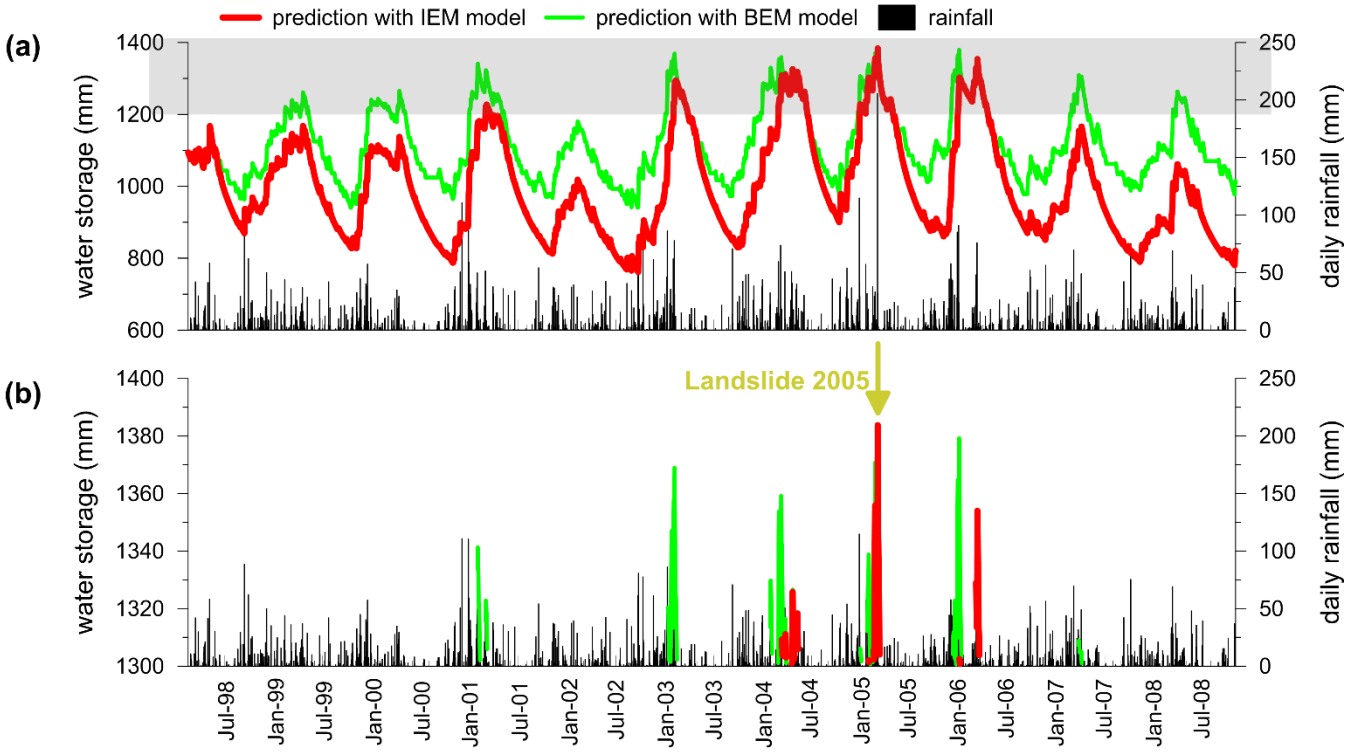

Figure 16: Comparison between IEM-predicted and BEM predicted evolutions of water storage, WS, for the layer involved in the 2005NIL: (a) prediction within the WS full range; (b) prediction for WS levels higher than 1300 mm.

Nat. Hazards Earth Syst. Sci. Discuss., https://doi.org/10.5194/nhess-2017-285
Manuscript under review for journal Nat. Hazards Earth Syst. Sci.
Discussion started: 7 September 2017

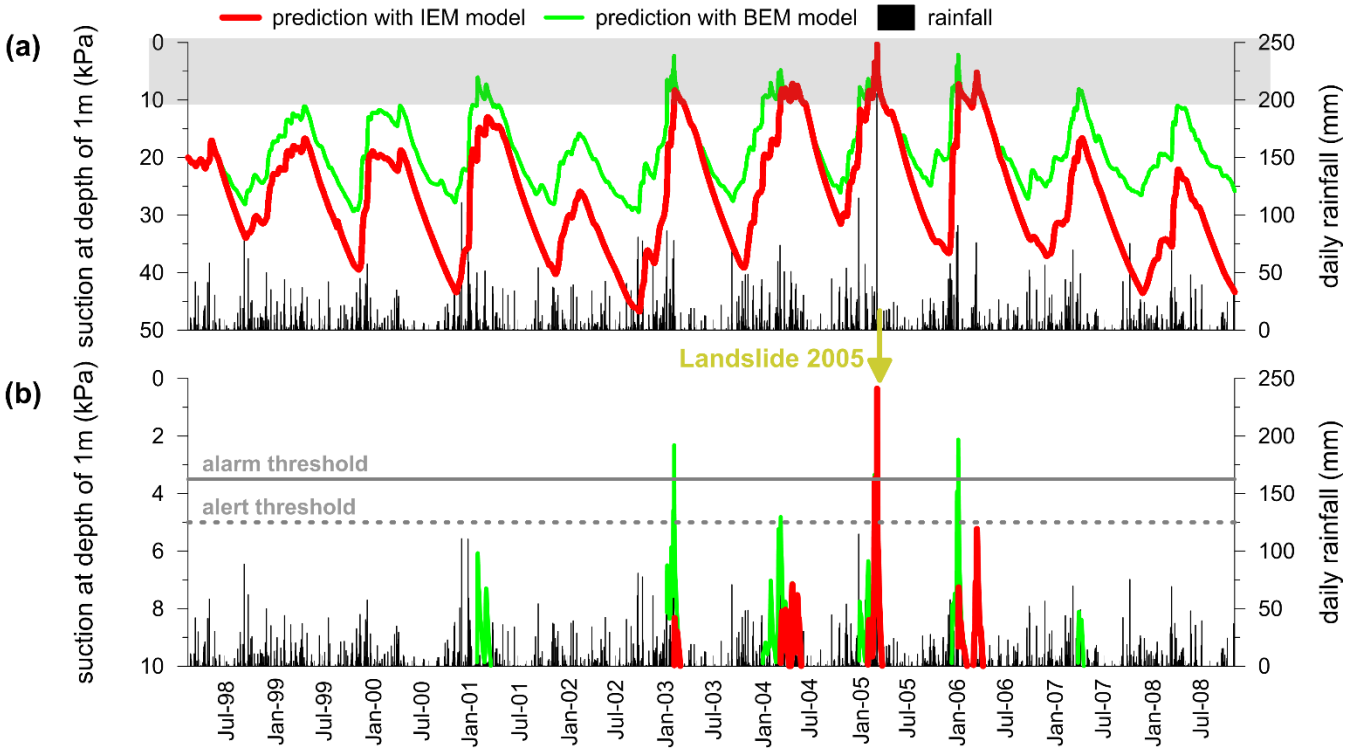

Figure 17: Comparison between IEM-predicted and BEM predicted evolutions of suction for the layer involved in the 2005NIL: (a) prediction within the suction full range; (b) prediction for suction levels lower than 10 kPa.

Nat. Hazards Earth Syst. Sci. Discuss., https://doi.org/10.5194/nhess-2017-285
Manuscript under review for journal Nat. Hazards Earth Syst. Sci.
Discussion started: 7 September 2017

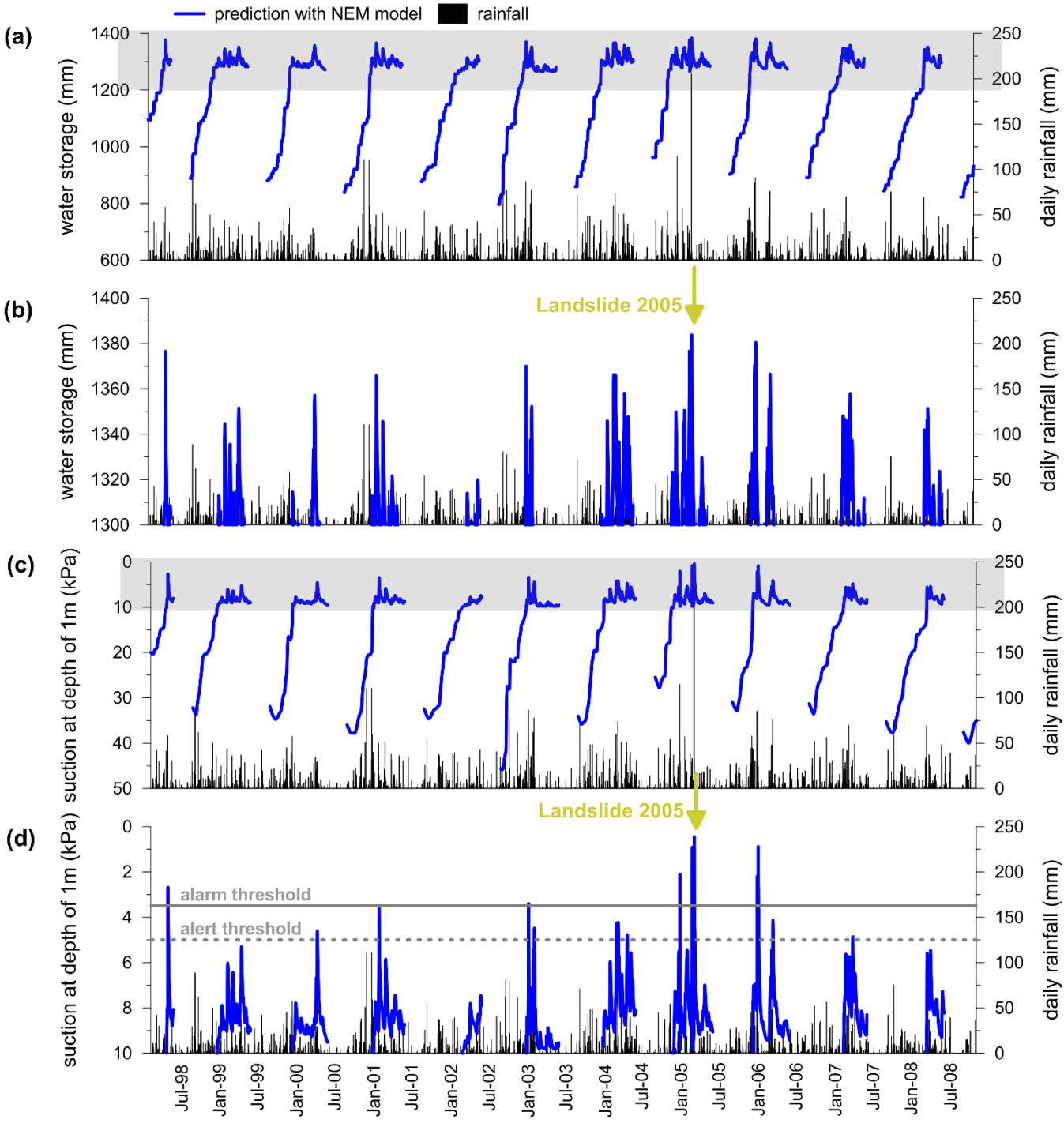

Figure 18: NEM prediction of the hydrological behaviour evolution for the layer involved in the 2005NIL: (a) prediction within the WS full range; (b) prediction for WS levels higher than 1300 mm; (c) prediction within the suction full range; (d) prediction for suction levels lower than 10 kPa.